RSC Advances

PAPER

View Article Online
View Journal | View Issue

Cite this: *RSC Adv.*, 2025, **15**, 37371

Effect of current collectors on the electrochemical performance of semi-solid $LiFePO_4$ lithium slurry batteries

Nabil El Halya,† Yassine Seffar,† Mohamed Aqil, Jones Alami and Mouad Dahbi *

Semi-solid lithium slurry batteries represent an innovative energy storage technology that simplifies manufacturing, reduces costs, and enhances safety, and recyclability. Beyond the intrinsic conductivity of the slurry, their performance is strongly governed by the interfacial contact resistance between the slurry and the current collector. The nature and structure of the current collector critically influence electron transport, polarization losses, and overall electrochemical stability. Here, we investigate the electrochemical performance of three current collector types (aluminum metal, carbon felt, and carbon cloth) in $LiFePO_4$ based semi-solid lithium slurry batteries. Our findings reveal that carbon cloth outperforms the other collectors, achieving 95% capacity retention after 100 cycles at 1 C and delivering a high capacity of 70 mA h g^{-1} at 10 C. Notably, even under high-loading conditions, carbon cloth maintains superior electrochemical performances. This study highlights the pivotal role of current collectors in semi-solid lithium slurry battery performance, offering a promising pathway toward scalable, high-efficiency energy storage solutions.

Received 31st August 2025
Accepted 26th September 2025

DOI: 10.1039/d5ra06521f

rsc.li/rsc-advances

Introduction

As fossil fuel supplies decrease, renewable energy sources like solar and wind power have seen rapid growth in recent years. To keep the power grid stable and improve energy efficiency, reliable energy storage systems are needed. However, solar and wind power are not always stable or continuous, which makes it difficult to integrate them smoothly into energy storage grids.[1–4] Lithium-ion batteries (LIBs), known for their high energy density,[5–9] are now widely used for energy storage. But as the size of energy storage systems, such as large power stations, increases, the cost of LIBs becomes a major concern. More battery modules are needed, which raises not only the cost of the batteries but also the cost of designing the modules. This results in high initial investment for large-scale energy storage projects.

Unlike traditional lithium-ion batteries with fixed and bonded electrodes, semi-solid lithium slurry batteries (SSLSBs) use a mixture of solid and liquid materials for some or all of the electrodes.[10,11] This design eliminates the need for traditional lithium-ion battery electrode manufacturing steps such as coating, drying, and thermal pressing, simplifying the production process and reducing production costs significantly. It also prevents issues like capacity loss and cycle life degradation caused by electrode material detachment or loosening. Furthermore, the innovative technology in SSLSBs allows for the online repair of microstructures at the battery's internal interfaces, making it a low-cost, long-life, high-safety, and easily recyclable energy storage technology.

SSLSBs refers to a lithium battery technology where all or part of the electrodes are composed of a slurry containing active materials, conductive agents, and electrolyte. Currently, two forms of SSLSBs technologies have been developed: the external circulation system and the non-external circulation system.[12,13] The external circulation SSLSBs combines the high energy density of traditional lithium batteries with the flexible and scalable structure of flow batteries, primarily intended for applications in large-capacity energy storage fields such as grid energy storage. However, this configuration continues to suffer from substantial pumping losses and flow-dependent transport limitations. These challenges are primarily driven by the high viscosity associated with elevated solid loadings and the formation of diffusion-limited particle clusters comprising active materials and conductive additives, which obstruct flow channels, increase pumping losses, and ultimately reduce efficiency.[14,15] The hydrodynamics of slurry electrodes are strongly influenced by the physicochemical characteristics of the active particles, including size, shape, surface morphology, and composition as well as the operational parameters, such as flow rate, pressure gradients, and channel architecture. Consequently, a comprehensive understanding of shear-induced mass transport, non-Newtonian rheology, shear-dependent electronic conductivity, and associated parasitic losses is

Materials Science, Energy and Nano-engineering Department, Mohammed VI Polytechnic University, Ben Guerir, Morocco. E-mail: Mouad.dahbi@um6p.ma
† Authors contribute equally.

essential to optimize performance and enable high-efficiency semi-solid electrochemical systems.[16–18]

On the other hand, the non-external circulation system of lithium slurry batteries does not consider issues like slurry viscosity and mechanical losses due to circulation drive and achieves high energy density by increasing the loading of active materials in the electrode slurry.[19–21] In SSLSBs, besides being influenced by the conductivity of the electrode slurry itself, polarization is also affected by the contact resistance at the interface between the slurry and the current collector. The choice of current collector plays a critical role in determining electrochemical performance because the slurry is not rigidly bound, and the interfacial contact resistance between the slurry and the collector becomes a key limiting factor. Planar metallic foils such as aluminum provide only a two-dimensional interface with limited anchoring, often resulting in poor slurry adhesion and higher interfacial resistance. In contrast, three-dimensional porous current collectors, such as carbon felt and carbon cloth, enable slurry infiltration into their pore networks, significantly enhancing electronic connectivity and ionic accessibility. This structural difference leads to dual transport pathways: electrons are conducted through the interconnected carbon framework, while the porous architecture accommodates slurry penetration and facilitates ionic transport, resulting in more homogeneous electrochemical reactions.

Lestriez *et al.*[22] compared the electrochemical impedance spectra of $Li_4Ti_5O_{12}$ (LTO) semi-solid batteries under two scenarios: using the same current collector with different electrode slurries and using different current collectors with the same electrode slurry. The study found that the charge transfer resistance in the electrochemical impedance spectroscopy (EIS) spectrum mainly originates from the interface contact resistance between the slurry and the current collector. Moreover, the higher the grit number of the sandpaper used to polish the current collector surface, the smaller the measured charge transfer resistance. Additionally, Morante *et al.*[23] compared the EIS spectra of $LiNi_{1/3}Co_{1/3}Mn_{1/3}O_2$ slurry cells using aluminum plate current collectors and titanium plate current collectors. They found that when the current collector changed from aluminum to titanium, the charge transfer impedance increased from 150 Ω to 300 Ω, indicating that the material of the current collector also affects the interface resistance.

In order to improve the current collection characteristics of thick electrode slurry and reduce battery polarization, the literature mainly employs surface plating or coating modifications on the current collector,[24] or directly uses porous foam metals,[25–27] three-dimensional carbon materials,[28,29] *etc.* However, from the reported charge transfer resistance values in the literature, only foam metals and three-dimensional carbon materials have lower internal resistance for current collection. Moreover, Tarascon *et al.*[30] studied the cyclic voltammetry curves of $LiFePO_4$ (LFP)/Li half-cells using an aluminum plate as the current collector with a 1 mm slurry thickness and foam aluminum as the current collector with a 6 mm slurry thickness. The results showed that although the latter increased the slurry thickness six-fold, the oxidation and reduction peaks of the cells under both structures were similar, indicating that the use of foam aluminum effectively compensated for the increased internal resistance caused by the thicker slurry. Another group tested the charge and discharge performance of a half-cell using a 1 mm thick LFP slurry (19 wt% LFP-1.9 wt% KB) with carbon felt as the current collector.[28] They found that the polarization of the cell is lower when using three-dimensional carbon felt material. Nevertheless, since the three-dimensional conductive material's matrix often occupies a large volume fraction, the effective volume that the slurry can occupy within the pores is reduced, limiting the cell capacity. Excessive use would also increase the weight of non-active materials in the battery, reducing its energy density and not being favorable for practical applications. Herein, carbon with a three-dimensional (3D) interconnected architecture holds promise as a potential candidate due to its high surface area, which enhances contact with active materials and promotes greater interfacial interaction compared to flat current collectors and allows active particles to occupy a larger space while ensuring a good conductivity network.[31] This mitigates the limitations of energy density and electron transport resistance. Various 3D carbon matrices have been used as current collectors in slurry-based LiBs, including carbon cloth, carbon fiber, and carbon felt. Each type of carbon results in different behaviors of the same active material. For instance, Hongning Chen *et al.*[32] reported that the LFP capacity increases when using carbon felt instead of carbon cloth. The morphology and design of the current collector are crucial parameters in slurry-based LiBs, significantly affecting the actual battery capacity and its stability during long-term cycling.

Carbon cloth and carbon felt are emerging as promising current collectors for lithium slurry batteries due to their excellent stability, conductivity, and uniformity. The structure of carbon cloth provides robust flexibility, ensuring strong contact with the slurry while resisting handling-induced deformation-critical factors for consistent performance. Additionally, carbon cloths offer stable and uniform conductivity, facilitating efficient electron flow and balanced current distribution. On the other hand, carbon felt typically features a more porous structure than carbon cloth, offering a higher surface area that enhances interactions with electrolytes and active materials. The structural integrity and durability of both materials make them dependable choices for long-term, high-performance applications in lithium slurry batteries. This study aims to evaluate and compare the performance of aluminum metal, carbon cloth and carbon felt as current collectors in LFP-based SSLSBs, highlighting their potential to enhance battery efficiency, durability, and practical applicability.

Experimental

LFP slurry preparation

The cathode slurry was formulated inside the glovebox through the following procedure: initially, 25 w% of LFP and 5 w% of carbon black were mixed in a 20 ml small pot. This mixture was then subjected to ball milling at 1700 rpm for 10 minutes,

employing zirconia balls, to ensure good mixing. Subsequently, 70 w% of electrolytes (1 M $LiPF_6$ in EC/DMC) were introduced and mixed.

Preparation of LFP-based half slurry battery

The electrochemical performance of LFP catholyte was evaluated using a CR2025 coin cell. Three types of current collectors (aluminum metal, carbon felt and carbon cloth) were attached to the coin cell with an LFP loading of 3–5 mg cm^{-2} for low loading electrodes and 15–18 mg cm^{-2} for high loading electrodes. Whatman and lithium metal were used as separators and counter electrode respectively.

Assembly of LFP and LTO full cell

Similarly to half-cell assembly, the current collector was attached to the positive shell and loaded with about 30 mg of LFP slurry. The loading of the anolyte was calculated according to N/P $\sim$ 1.1. The LFP||LTO cells were assembled inside the glove box.

Material characterizations

The crystal structure and morphology of LFP and current collectors were thoroughly characterized through X-ray diffraction (XRD) using a BRUKER D8 ADVANCE diffractometer with Cu Kα radiation, Raman spectroscopy with a LabRAM 300 Raman spectrometer (Horiba Jobin Yvon), and Scanning Electron Microscopy (SEM) on a ZEISS EVO 10 microscope.

Electrochemical measurements

EIS and cyclic voltammetry (CV) measurements were conducted using an MPG-2 potentiostat (Bio-Logic SAS). CV experiments were performed at scan rates ranging from 0.05 to 2 mV s^{-1} within a voltage window of 2.5 to 3.9 V (*vs.* Li^+/Li). Galvanostatic charge/discharge tests were conducted within the same voltage range.

Results and discussion

Before assessing the electrochemical performance of the SSLSBs, a comprehensive structural analysis was conducted on the as-received commercial LFP particles. The XRD pattern shown in Fig. S1a reveals diffraction peaks at 17.12°, 20.75°, 25.52°, 29.68°, 32.16°, 35.52°, and 52.42°, which match precisely with the reference pattern of olivine-phase LFP (PDF#40–1499).[33,34] Notably, no secondary phases or impurities were detected, indicating the high phase purity of the material.

Raman spectroscopy is carried out to identify the surface chemical composition and assessing the degree of graphitization in carbon-based LFP/C composites.[35–38] The Raman spectrum presented in Fig. S1b exhibits two characteristic peaks at 1325 cm^{-1} and 1593 cm^{-1}, corresponding to the D band (disordered carbon, sp^3) and G band (graphitic carbon, sp^2), respectively, which are indicative of the carbon's structural order.[37] The calculated intensity ratio (ID/IG) of 0.9 reflects a considerable presence of graphitic carbon, which is advantageous for improving the electronic conductivity of the LFP matrix.[36,39] Furthermore, a peak at 948 cm^{-1} is observed, attributed to the intramolecular stretching vibration of the PO_4^{3-} anion.[37]

The SEM images of LFP particles presented in Fig. S1c reveal a highly porous, interconnected nanoparticle structure, offering extensive surface area and pathways conducive to efficient ion and electron transport. Moreover, the EDX images show a homogeneous distribution of oxygen, phosphorus, and iron, reflecting a uniform composition.

Fig. 1 presents the SEM images of carbon cloth and carbon felt current collectors. The SEM images of carbon cloth (Fig. 1a–c) depict a well-organized, tightly woven structure with smooth, cylindrical fibers arranged in a dense, interconnected network. This ordered architecture promotes uniform slurry infiltration, ensuring stable conductive contact across the material. The close inter-fiber spacing and regular alignment facilitate efficient electron flow and consistent current distribution, minimizing polarization effects and enhancing battery performance.

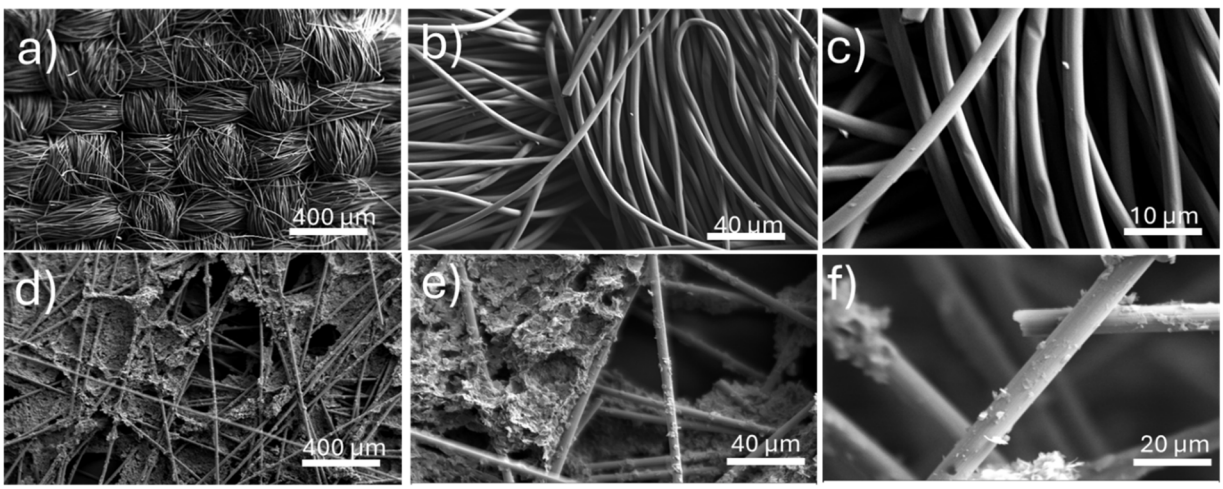

Fig. 1 SEM images of carbon cloth (a–c) and carbon felt (d–f) current collectors.

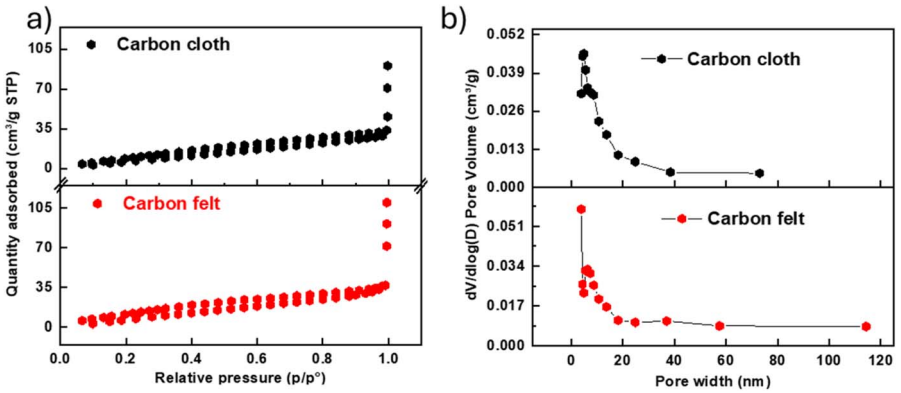

Fig. 2 N_2 adsorption–desorption isotherms (a) and pore size distribution (b) of carbon cloth and carbon felt current collectors.

In contrast, the SEM images of carbon felt (Fig. 1d–f) show a disordered network of loosely arranged fibers with a rough, irregular surface. This random structure creates significant gaps between fibers, which hinders uniform slurry infiltration and consistent conductive pathways throughout the material. As a result, carbon felt as a current collector may suffer from non-uniform electron transport and uneven current distribution, potentially leading to increased polarization and reduced overall performance and stability of the lithium slurry batteries.

The N_2 adsorption–desorption isotherms and pore size distributions are presented in Fig. 2a and b. The isotherm curves display a hysteresis loop in the relative pressure range of 0.1–0.9, consistent with type IV isotherms as classified by the IUPAC. The pore size distribution curves indicate a predominance of mesopores in both carbon felt and carbon cloth samples.[40,41] BET analysis reveals a moderate specific surface area, reflecting a combination of microporosity and interparticle mesoporosity, while BJH pore size distribution confirms predominantly uniform mesopores (2–50 nm), advantageous for ion transport and electrolyte accessibility. Metallic current collectors, such as aluminum, show negligible adsorption and no pronounced hysteresis, indicating a nearly non-porous structure with very low surface area. While aluminum provides excellent electronic conductivity, its lack of intrinsic porosity limits electrolyte infiltration and ion transport, which may reduce electrochemical performance under high-rate conditions.

Electrochemical performances of LFP slurry

For electrochemical characterization, the lithiation/delithiation behavior of LFP-based lithium slurry batteries with different current collectors were examined using cyclic voltammetry within the voltage window of 2.5–3.9 V at a scan rate of 0.05 mV s^{-1}. As depicted in Fig. 3, carbon cloth exhibits superior electrochemical behavior, with sharp oxidation and reduction peaks at 3.55 V and 3.32 V, respectively, and the smallest hysteresis, indicating low polarization and high reversibility. The aluminum metal shows intermediate performance, with peaks at 3.52 V and 3.33 V and moderate hysteresis. In contrast, carbon felt demonstrates the largest hysteresis, with oxidation and reduction peaks at 3.50 V and 3.35 V, suggesting higher internal resistance and reduced reversibility.

Cycling tests were conducted at 0.1 C rate (1 C = 170 mA g^{-1}) within a voltage range of 2.5–3.9 V. Fig. 4a, d and g presents the discharge/charge profiles of LFP-based lithium slurry batteries using different current collectors. Across all current collectors, the discharge/charge profiles exhibit two distinct plateaus at 3.45 V and 3.40 V, corresponding to the delithiation and lithiation processes of LFP, respectively. Furthermore, all current collectors demonstrate an excellent initial coulombic efficiency of 99.4%, minimal hysteresis, and a first discharge capacity of 162 mA h g^{-1}.

Fig. 4b, e and h illustrate the long-term cycling performance of the different current collectors tested at a 1 C rate over 100 cycles. The carbon cloth exhibits a higher first discharge capacity of 157 mA h g^{-1} compared to 135 mA h g^{-1} for the aluminum metal and 134 mA h g^{-1} for the carbon felt. Furthermore, the carbon cloth demonstrates superior capacity retention of 95% after 100 cycles, outperforming the aluminum metal and carbon felt, which retain 91% and 85%, respectively. This enhanced performance of the carbon cloth can be attributed to its highly conductive and flexible structure, which minimizes internal resistance during repeated cycling. In contrast, the carbon felt undergoes greater structural degradation during cycling, leading to its reduced capacity retention.

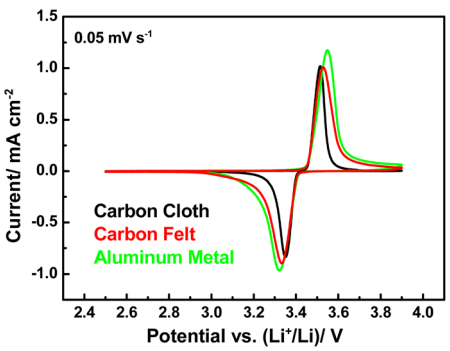

Fig. 3 Cyclic voltammetry curves of LFP based lithium slurry batteries using different current collectors.

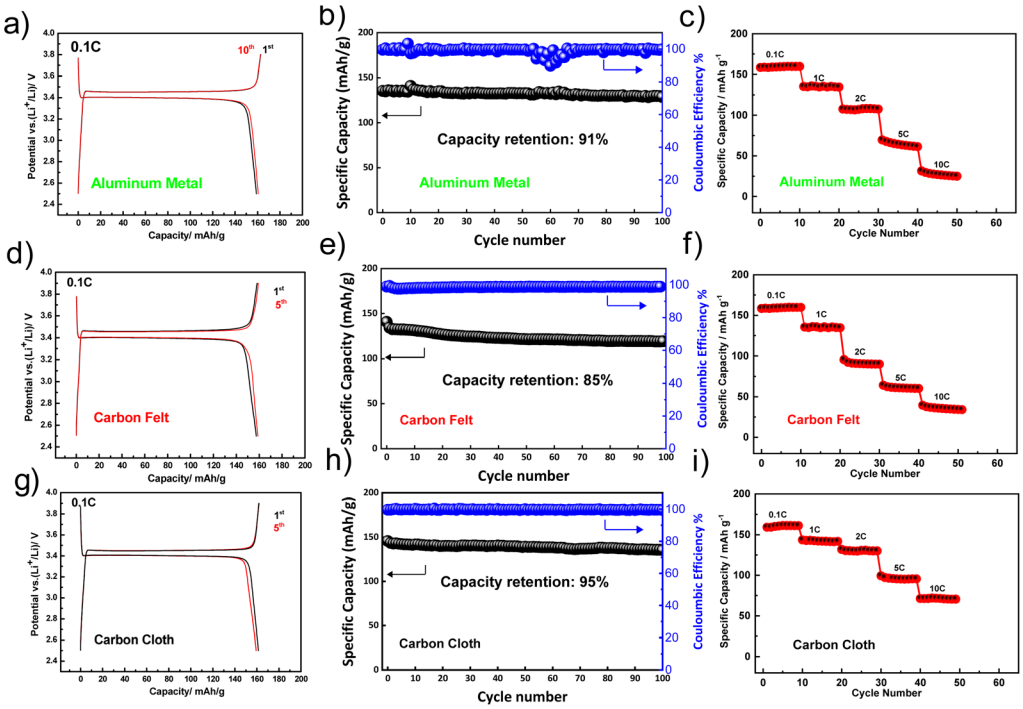

Fig. 4 Charge/discharge profile (a, d and g), long term cycling at 1 C (b, e and h) and rate capability performance (c, f and i) of LFP based SSLSBs using aluminum metal, carbon felts and carbon cloths current collectors.

Fig. 4c, f and i presents the rate capability profiles of the three current collectors at various current rates, from 0.1 C to 10 C, within a voltage range of 2.5–3.9 V. The carbon cloth current collector exhibits a reversible capacity of 164 mA h g^{-1} at 0.1 C and 150 mA h g^{-1} at 1 C. At a high rate of 10 C, it maintains a capacity of 70 mA h g^{-1}, with a capacity retention of 65% after 1000 cycles (Fig. S2). In comparison, the aluminum metal and carbon felt show a similar reversible capacity of 160 mA h g^{-1} at 0.1 C but drop to only 130 mA h g^{-1} at 1 C and 20 mA h g^{-1} at 10 C. The superior high-rate performance of carbon cloth is primarily attributed to its highly conductive and mechanically flexible woven structure, which promotes efficient electron transport while maintaining robust electrode–slurry interfacial contact under high current densities. SEM images of the carbon cloth and carbon felt current collectors after 100 cycles at 1 C (Fig. S3) reveal that carbon cloth preserves its woven morphology even after extended cycling, exhibiting only minor surface deposits, indicative of its excellent structural integrity and stable electrode–current collector interface. In contrast, carbon felt displays significant accumulation of dense slurry residues and particle agglomerates on its surface, leading to pore blockage and restricted ion transport pathways. This morphological degradation contributes to increased interfacial resistance and explains the more pronounced capacity decay observed for carbon felt during high rate cycling. Collectively, these observations underscore the critical role of current collector architecture in sustaining electrochemical performance in semi-solid lithium slurry batteries.

Fig. 5 presents the EIS profiles of LFP based SSLSBs employing the different current collectors after one cycle at 0.1 C. The Nyquist plots reveal that the cell with carbon cloth exhibits the smallest semicircle diameter, indicating the lowest charge-transfer resistance and suggesting superior electronic conductivity and interfacial charge-transfer kinetics. In contrast, carbon felt displays the largest semicircle, reflecting significant resistive losses and pronounced interfacial polarization. These findings are consistent with the low-capacity retention observed for the carbon-felt-based SSLSB (Fig. 4).

The EIS spectra were fitted using the equivalent circuit R_1–(R_2||C_1)–(R_3||C_2)–W, where R_1 denotes the ohmic resistance, R_2||C_1 represents a fast interfacial or surface-film process, R_3||C_2

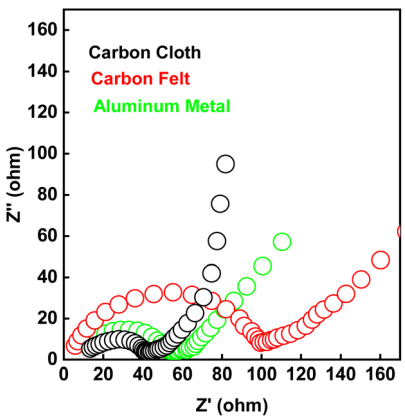

Fig. 5 Nyquist plot of LFP based semi-solid battery using aluminum metal, carbon felt and carbon cloth current collectors after one cycle at 0.1 C.

corresponds to the charge-transfer process, and W is the Warburg diffusion element (Fig. S4). Among the tested electrodes, carbon cloth delivers the lowest charge-transfer resistance ($R_3 =$ 18.66 Ω), which is 19% and 44% lower than those of aluminum (23.07 Ω) and carbon felt (33.07 Ω), respectively, indicating faster interfacial kinetics and a higher exchange current. The series resistance (R_1) also varies across electrodes, reflecting differences in their structural and electrical properties. Despite its high intrinsic conductivity, aluminum exhibits a relatively high R_1 due to limited contact with the slurry caused by its smooth and compact surface. Carbon felt, composed of loosely packed, tortuous fibers, promotes slurry infiltration but suffers from reduced bulk conductivity, resulting in the highest R_1. Carbon cloth, with its interconnected fiber network, ensures both efficient electron transport and intimate slurry contact, yielding an intermediate R_1 (12.57 Ω).

The interfacial resistance (R_2) remains comparable across electrodes (52–59 Ω). Although carbon cloth shows the highest Warburg coefficient ($S_1 = 27.24\ \Omega\ s^{-1/2}$), indicative of slightly more pronounced mass-transport limitations at low frequencies, the significant reduction in R_3 dominates the overall impedance response. Consequently, the total resistive contribution ($R_1 + R_2 + R_3$) is the lowest for carbon cloth (90 Ω), compared with carbon felt (93.9 Ω) and aluminum (98.6 Ω). As a result, the carbon-cloth current collector delivers the most favorable electrochemical performance despite its modestly higher diffusion impedance.

Fig. 6 compares the performance of the LFP-based SSLSBs using carbon felt and carbon cloth current collectors with an electrode loading of 15 mg.cm^{-2}. The battery with carbon felt shows more voltage polarization and faster capacity fade, likely due to poor contact with the slurry and limited electron and ion transport. In contrast, the battery with carbon cloth presents lower polarization, higher discharge capacity, and slower capacity loss over cycling. This suggests that carbon cloth provides better contact with the slurry and more efficient pathways for electron and ion movement, making it a more effective current collector for high-loading conditions.

LFP Slurry was then assembled into a coin-type full cell using commercial LTO. The LTO based slurry battery presents a capacity of 160 mA h g^{-1} at 0.1 C and excellent stability after 100 cycles at 1 C (Fig. S3). Fig. 7a is a schematic illustration of the LFP/LTO slurry full cell. As shown in Fig. 7b, there is only a pair of distinct oxidation peaks (1.89 V) and reduction peaks (1.83 V) in the dQ/dV spectrum of LFP/LTO with a minimal overvoltage of 0.06 V, indicating excellent electrode kinetics and high reversibility. The dq/dv peaks show that the full cell potential is 1.86 V matching the voltage difference between LTO and LFP. Fig. 7c and d shows the first charge/discharge cycle at 0.1 C (1 C = 170 mA.g^{-1}) in a voltage range of 0.5–3 V. The full cell delivers a capacity of 140 mA h.g^{-1} (based on the mass of LFP) with excellent reversibility and minimal capacity fading. This result illustrates the high electrochemical performance, stability, and potential applicability of the LFP slurry full cell in practical energy storage systems.

Conclusions

This study highlights the critical role of current collectors in the performance of LFP based lithium slurry batteries. Among the three types studied (aluminum metal, carbon felt, and carbon cloth) carbon cloth demonstrated superior performance,

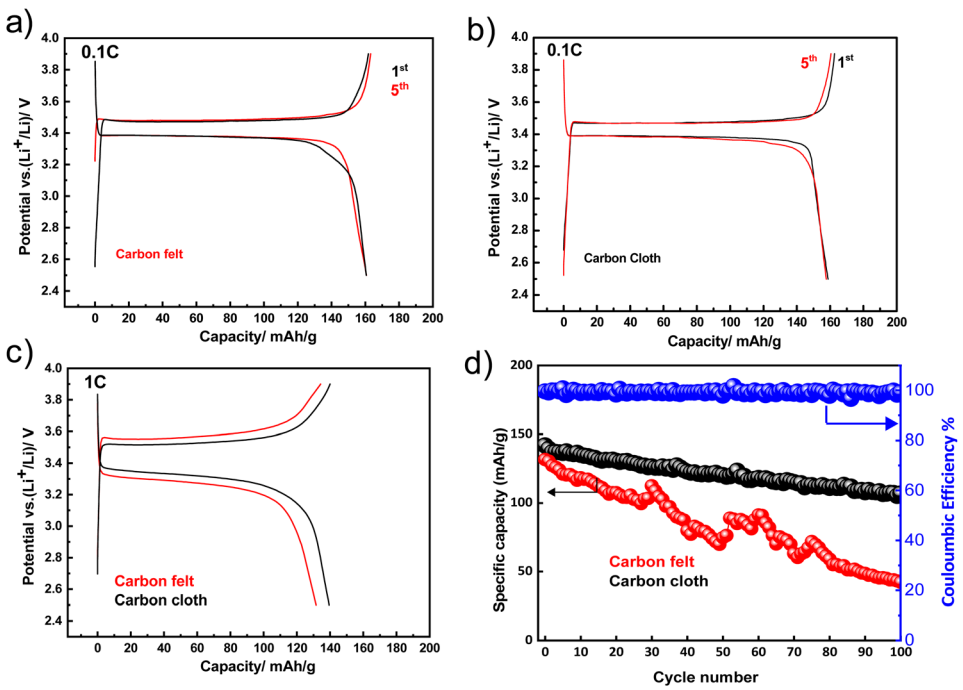

Fig. 6 Charge/discharge profile at 0.1 C (a and b) and long-term cycling at 1 C (c and d) of carbon felt and carbon cloths current collectors.

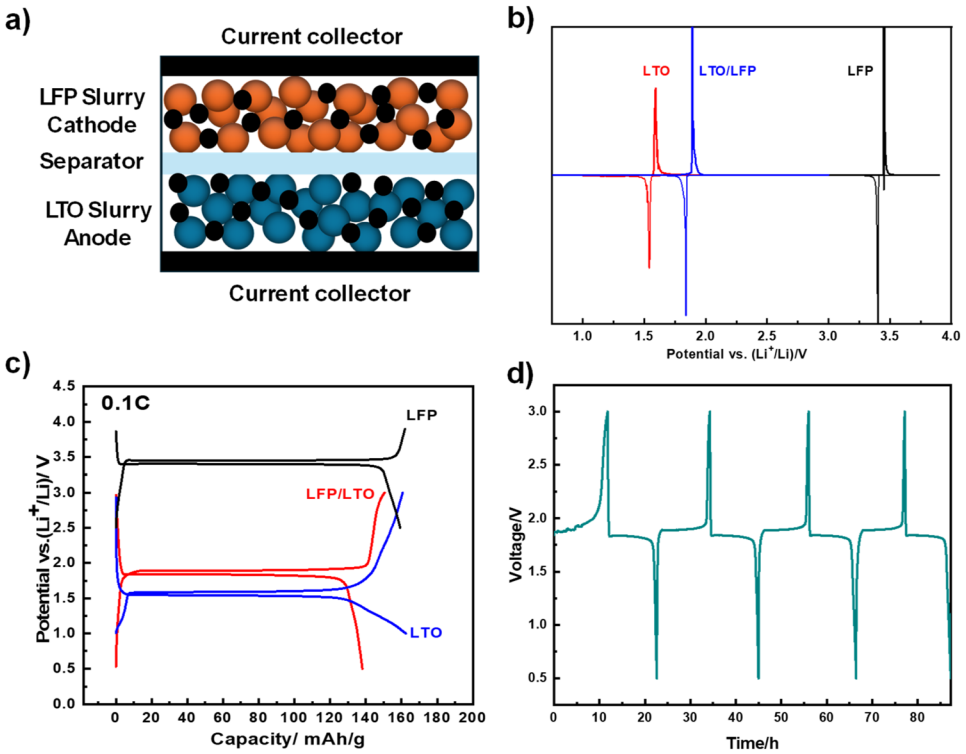

Fig. 7 Schematic illustration of the LFP based lithium slurry full cell (a). Differential capacity plots, dQ/dV *vs.* voltage, for the first cycle of LTO, LFP and the full cell (b). Galvanostatic charge–discharge profiles of LFP||LTO (c and d).

achieving 95% capacity retention after 100 cycles at 1 C and maintaining a high discharge capacity of 70 mA h g^{-1} at 10 C. This exceptional performance, even under high-loading conditions, is attributed to the carbon cloth's 3D architecture, which enhances interfacial contact and mitigates polarization losses. While carbon cloth exhibits superior electrochemical performance, its higher material cost and more complex manufacturing process pose challenges for large-scale implementation. Although its structure minimizes polarization and maintains high-capacity retention even under high-loading conditions, practical adoption in commercial lithium slurry batteries requires balancing performance with cost and scalability. Future strategies to address these limitations could include optimizing the carbon cloth production process to reduce material consumption and developing hybrid or composite current collectors that combine carbon cloth with lower-cost substrates. These approaches aim to retain the electrochemical advantages of carbon cloth while minimizing cost and maintaining mechanical durability. By considering both mechanistic performance and practical feasibility, such strategies can facilitate the translation of laboratory-scale improvements into commercially viable, large-scale energy storage solutions.

Author contributions

Nabil El Halya: idea conception, experimental investigation and writing of the original draft. Yassine Seffar: formal analysis, experimental part, Mohamed Aqil: review and editing, Mouad Dahbi and Jones Alami: conceptualization, validation, review & editing, funding acquisition.

Conflicts of interest

The authors declare that they have no known competing financial interests or personal relationships that could have appeared to influence the work reported in this paper.

Data availability

All data supporting the findings of this study are provided in the main manuscript and the accompanying supplementary information (SI). Supplementary information is available. See DOI: **https://doi.org/10.1039/d5ra06521f**.

Acknowledgements

The authors would like to thank Office Chérifien des Phosphates (OCP S.A.) and Mohammed VI Polytechnic University for financial support.

References

1 N. El Halya, M. Tayoury, M. Aqil, A. Aboulaich, R. Amine, F. Ghamouss, M. Makha, J. Alami and M. Dahbi, *Sustain. Energy Fuels*, 2024, **8**, 2330–2356.
2 S. Cheng, Y. Hu, L. Jiang, H. Dang, Y. Ding, Q. Duan, H. Xiao, J. Sun and Q. Wang, *Fire Technol.*, 2023, **59**, 1181–1197.

3 A. Masmoudi, A. Abdelkafi and L. Krichen, *Energy*, 2011, **36**, 5016–5026.
4 T. Niknam, A. Kavousifard, S. Tabatabaei and J. Aghaei, *J. Power Sources*, 2011, **196**, 8881–8896.
5 N. El Halya, K. Elouardi, A. Chari, A. El Bouari, J. Alami and M. Dahbi, in *Titanium Dioxide - Advances and Applications*, IntechOpen, 2022.
6 N. El Halya, M. Kerroumi, E. H. Elmaataouy, A. Amarray, M. Aqil, J. Alami and M. Dahbi, *RSC Adv.*, 2023, **13**, 34416–34426.
7 N. El Halya, M. Aqil, K. El Ouardi, A. Bano, A. El Bendali, L. Hdidou, R. Amine, S. Son, F. Ghamouss, D. T. Major, K. Amine, J. Alami and M. Dahbi, *Batter Supercaps*, 2024, **7**(1), e202300424.
8 E. Elmaataouy, A. Chari, A. El Bendali, M. Tayoury, R. Amine, M. Aqil, G. Xu, T. Liu, J. Alami and M. Dahbi, *Batteries*, 2022, **9**, 23.
9 E. ELmaataouy, M. EL Kassaoui, M. ELmouhinni, K. Kubota, A. Chari, M. Aqil, A. Sghiouri, J. Alami, O. Mounkachi and M. Dahbi, *ChemSusChem*, 2025, **18**, e202500300.
10 C. Feng, Y. Chen, D. Liu and P. Zhang, *IOP Conf. Ser. Mater. Sci. Eng.*, 2017, **207**, 012076.
11 M. Duduta, B. Ho, V. C. Wood, P. Limthongkul, V. E. Brunini, W. C. Carter and Y. Chiang, *Adv. Energy Mater.*, 2011, **1**, 511–516.
12 M. Park, J. Ryu, W. Wang and J. Cho, *Nat. Rev. Mater.*, 2016, **2**, 16080.
13 K. B. Hatzell, M. Boota and Y. Gogotsi, *Chem. Soc. Rev.*, 2015, **44**, 8664–8687.
14 K. C. Smith, Y.-M. Chiang and W. Craig Carter, *J. Electrochem. Soc.*, 2014, **161**, A486–A496.
15 T. S. Wei, F. Y. Fan, A. Helal, K. C. Smith, G. H. McKinley, Y. M. Chiang and J. A. Lewis, *Adv. Energy Mater.*, 2015, DOI: **10.1002/aenm.201500535**.
16 Y. Wang and J. G. Brasseur, *AIChE J.*, 2019, **65**, e16617.
17 H. Parant, G. Muller, T. Le Mercier, J. M. Tarascon, P. Poulin and A. Colin, *Carbon*, 2017, **119**, 10–20.
18 G. Gao, S. Li, F. Liu, X. Wu and Y. Liu, *Energy Storage Sci. Technol.*, 2023, **12**, 329–338.
19 Z. Li, K. C. Smith, Y. Dong, N. Baram, F. Y. Fan, J. Xie, P. Limthongkul, W. C. Carter and Y.-M. Chiang, *Phys. Chem. Chem. Phys.*, 2013, **15**, 15833.
20 F. Y. Fan, W. H. Woodford, Z. Li, N. Baram, K. C. Smith, A. Helal, G. H. McKinley, W. C. Carter and Y.-M. Chiang, *Nano Lett.*, 2014, **14**, 2210–2218.
21 V. E. Brunini, Y.-M. Chiang and W. C. Carter, *Electrochim. Acta*, 2012, **69**, 301–307.
22 L. Madec, M. Youssry, M. Cerbelaud, P. Soudan, D. Guyomard and B. Lestriez, *J. Electrochem. Soc.*, 2014, **161**, A693–A699.
23 J. J. Biendicho, C. Flox, L. Sanz and J. R. Morante, *ChemSusChem*, 2016, **9**, 1938–1944.
24 T. Wei, F. Y. Fan, A. Helal, K. C. Smith, G. H. McKinley, Y. Chiang and J. A. Lewis, *Adv. Energy Mater.*, 2015, **5**(15), DOI: **10.1002/aenm.201570082**.
25 S. Hamelet, T. Tzedakis, J.-B. Leriche, S. Sailler, D. Larcher, P.-L. Taberna, P. Simon and J.-M. Tarascon, *J. Electrochem. Soc.*, 2012, **159**, A1360–A1367.
26 S. Hamelet, D. Larcher, L. Dupont and J.-M. Tarascon, *J. Electrochem. Soc.*, 2013, **160**, A516–A520.
27 X. Chen, B. J. Hopkins, A. Helal, F. Y. Fan, K. C. Smith, Z. Li, A. H. Slocum, G. H. McKinley, W. C. Carter and Y.-M. Chiang, *Energy Environ. Sci.*, 2016, **9**, 1760–1770.
28 C. Feng, Y. Chen, D. Liu and P. Zhang, *IOP Conf. Ser. Mater. Sci. Eng.*, 2017, **207**, 012076.
29 I. Ryu, J. W. Choi, Y. Cui and W. D. Nix, *J. Mech. Phys. Solid.*, 2011, **59**, 1717–1730.
30 S. Hamelet, T. Tzedakis, J.-B. Leriche, S. Sailler, D. Larcher, P.-L. Taberna, P. Simon and J.-M. Tarascon, *J. Electrochem. Soc.*, 2012, **159**, A1360–A1367.
31 S. Jin, Y. Jiang, H. Ji and Y. Yu, *Adv. Mater.*, 2018, **30**(48), 1802014.
32 H. Chen, Y. Liu, X. Zhang, Q. Lan, Y. Chu, Y. Li and Q. Wu, *J. Power Sources*, 2021, **485**, 229319.
33 G. Longoni, J. K. Panda, L. Gagliani, R. Brescia, L. Manna, F. Bonaccorso and V. Pellegrini, *Nano Energy*, 2018, **51**, 656–667.
34 L. Bao, G. Xu and M. Wang, *Mater. Charact.*, 2019, **157**, 109927.
35 X. Lou and Y. Zhang, *J. Mater. Chem.*, 2011, **21**, 4156.
36 Y. Xia, W. Zhang, H. Huang, Y. Gan, Z. Xiao, L. Qian and X. Tao, *J. Mater. Chem.*, 2011, **21**, 6498.
37 J. Qian, M. Zhou, Y. Cao, X. Ai and H. Yang, *J. Phys. Chem. C*, 2010, **114**, 3477–3482.
38 X. Zhou, F. Wang, Y. Zhu and Z. Liu, *J. Mater. Chem.*, 2011, **21**, 3353.
39 L.-X. Yuan, Z.-H. Wang, W.-X. Zhang, X.-L. Hu, J.-T. Chen, Y.-H. Huang and J. B. Goodenough, *Energy Environ. Sci.*, 2011, **4**, 269–284.
40 G. Lou, Y. Wu, X. Zhu, Y. Lu, S. Yu, C. Yang, H. Chen, C. Guan, L. Li and Z. Shen, *ACS Appl. Mater. Interfaces*, 2018, **10**, 42503–42512.
41 Y. Seffar, A. S. Idrissi, J. Alami and M. Dahbi, *ChemistrySelect*, 2025, **10**(23), e04368.